ACS OMEGA

http://pubs.acs.org/journal/acsodf

Article

Comparative Study on Pyrolysis Kinetics Behavior and High-Temperature Fast Pyrolysis Product Analysis of Coastal Zone and Land Biomasses

Jie Li, Yanchao Shang,[‖] Wei Wei, Zhengyi Liu,* Yingyun Qiao, Song Qin, and Yuanyu Tian

Cite This: *ACS Omega* 2022, 7, 10144−10155

Read Online

ACCESS | Metrics & More | Article Recommendations | Supporting Information

ABSTRACT: The pyrolysis characteristics of land biomass (corn stalks (Cs), pine sawdust (Ps)) and coastal zone biomass (Jerusalem artichoke stalks (JAs) and reed (Re)) were investigated based on thermogravimetric analysis (TGA) and products' analysis. The kinetic parameters were obtained by three isoconversional methods (Friedman, KAS, and FWO) and one model-fitting method (DAEM). The simultaneous effect of high temperature (700−900 °C) and high heating rate (1000 °C/s) on the pyrolysis product simulating the typical conditions of a fluidized bed gasifier was studied. TGA showed that high heating rates deepen the thermal cracking process of biomass. Compared with the land biomass, the initial decomposition temperature (T_i) of the coastal biomass is reduced significantly owing to its higher proportion of hemicellulose. These methods agree with the trends shown by the activation energy (E_a) distribution calculated, with fluctuations between 160 and 350 kJ/mol. The mean value activation energies of Re and JAs were higher than those of Cs and Ps between 10% and 90% conversion. The DAEM model showed that Cs and JAs have a good linear relationship between ln A and E_α during the main pyrolysis stage, while Ps and Re are relatively weaker. The kinetic compensation effect was evident for Cs and JAs during the main thermal cracking stage. Py-GC-MS results confirmed that phenols, hydrocarbons, PAHs, and oxygen heterocycle compounds were strongly present in the released volatile products. High-temperature fast pyrolysis of JAs produced a larger amount of PAH compounds than from Cs, Ps, and Re. A larger amount of hydrocarbons and phenols was generated from high-temperature fast pyrolysis of Ps. Some oxygen-containing volatiles are easily converted into aromatic products with higher stability under high temperature.

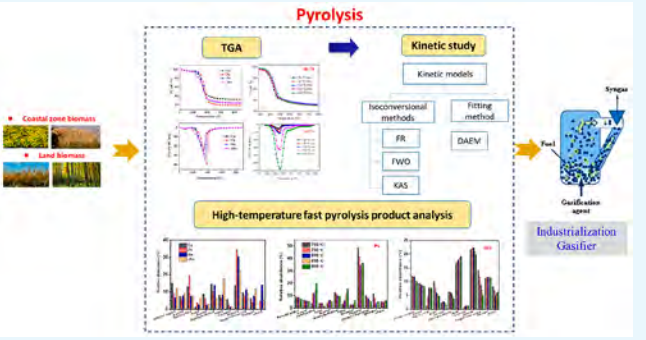

1. INTRODUCTION

The proposal of the "double carbon" goal has accelerated the development of multienergy integration and promoted the speed of replacing traditional fossil fuels with clean and green renewable energy.[1,2] Biomass energy, as the only green low-carbon resource among renewable energy, will play an important role in the future low-carbon energy structure because of its great potential in carbon reduction due to its capacity of carbon capture and storage (BECCS).[3] Gasification, as one of the most promising processes of large-scale, efficient, and clean utilization of biomass energy, can convert biomass with low energy density from solid state to high-grade combustible gas.[4] The fluidized bed gasifier is currently the main gasification technology at a large scale. The typical process conditions are as follows: high temperature (>700 °C), high heating rate (1000 °C/s), and short particle residence time (<5 s). The main advantage of this technology is the high conversion efficiency, and it can convert biomass into high yields of high-calorific-value gas products and tars with consistent chemical compositions through controlling factors.

Pyrolysis, as one of the most important stages of the biomass gasification process, directly determines the quality of gasification products. Pyrolysis is a thermochemical process in which occurs a series of physical changes and chemical reactions at 200−900 °C in the absence of air to produce gas, liquid (tars and condensable gases), and solid (char or coke) products.[5,6] The distribution of biomass pyrolysis products mainly depends on the properties of the feedstock and the parameters heating rate, reaction temperature, and residence time. Pyrolysis is beneficial to reduce pollutant emissions and utilize energy more efficiently and cleanly compared with combustion technology. In-depth study of the thermal

Received: November 11, 2021
Accepted: February 24, 2022
Published: March 15, 2022

decomposition properties of feedstocks is crucial for advancing gasification conversion.

Pyrolysis kinetics plays an extremely important role in the prediction of pyrolysis behavior and the rational design of the reactor in engineering applications, as kinetic analysis provides basic information on how materials decompose under different conditions.[7−9] The current thermal analysis methods are divided into isothermal methods and nonisothermal methods.[10] The isothermal method refers to the variation of the mass of a substance with time at a specific temperature, while the nonisothermal method refers to the variation of the substance under nonisothermal (usually linear heating) conditions. The isothermal method involves raising the temperature of the substance to be tested to near its decomposition temperature rapidly, which requires higher equipment accuracy and may also cause greater noise.[11] Compared with isothermal analysis methods, nonisothermal methods use temperature programming, which is less time-consuming and simple and has gradually become the main means of thermal analysis kinetics. Kinetic methods on nonisothermal solid-state reactions can be divided into two approaches: (i) isoconversional methods and (ii) model-fitting methods.[9,12−14] Compared to the model-fitting methods, the isoconversional methods can directly calculate the activation energy of the reaction without preassuming the $f(\alpha)$ mechanism function, which can avoid errors caused by assuming different mechanism functions.[10,15,16] Currently, there are many calculation models for isoconversional kinetics. These models can be categorized as differential methods and integral methods. The most popular isoconversional methods are the Friedman, Flynn−Wall−Ozawa (FWO) and Kissinger−Akahira−Sunose (KAS) methods.[7] The distributed activation energy model (DAEM) is a commonly used model-fitting method for calculating the kinetic parameters of pyrolysis reactions, which can describe the entire reaction process.[17] The DAEM assumes that the pyrolysis process of biomass proceeds through many independent parallel reactions with different activation energies, and the activation energy distribution of these reactions can be described by a continuous function.[18] With regard to biomass, this assumption is appropriate, because biomass is composed of a series of organic matter with extremely complex chemical structures and compositions, and these components have their own thermal decomposition behavior during the pyrolysis process. Várhegyi et al.[19] pointed out that the DAEM is the best model to describe the biomass devolatilization process.

In addition to the study of the kinetics of the pyrolysis of biomass, understanding the characteristics of the product is beneficial to the directional regulation of the pyrolysis process and obtaining high yields of high-calorific-value gas products and tars with consistent chemical compositions. The heating rate and temperature affect the chemical properties of the primary pyrolysis product by affecting the rate of biomass devolatilization and then determine the eventual biomass pyrolysis product.[20] At present, a large number of literature reports pay attention to the fast pyrolysis process of biomass for the production of liquid fuel at low temperature (400−600 °C).[21−24]

The coastal zone is a narrow interface zone between marine and terrestrial areas.[25] The coastal zone resource is an important reserve land resource with dynamic growth. Its reasonable development is an effective way to alleviate the dual pressure of population growth and cultivated land reduction in coastal areas, and it has very important practical significance to promote the economic development of coastal areas.[26] Jerusalem artichoke (*Helianthus tuberosus L.*) and reed are two common salt tolerant plants in the coastal zone.[27,28] In China, the annual production of Jerusalem artichoke and reed in the coastal zone is about 800 million tons.[29]

Up to now, no satisfactory information has been found in the literature about the pyrolysis kinetic behavior and a detailed analysis of the reaction products under the simultaneous effects of high temperature and high heating rate for land and coastal biomass. Therefore, this paper aims to (1) explore the effects of heating rates (50, 80, 100, 300, and 600 °C/min) and feedstock properties on the thermal behavior and mechanism by thermogravimetric analysis, (2) calculate the pyrolysis kinetic parameters of coastal waste biomass by isoconversional (Friedman, FWO, and KAS) methods and the DAEM, and (3) investigate the simultaneous effects of high temperature (700−900 °C) and high heating rate (1000 °C/s) on the pyrolysis product, simulating the typical conditions of a fluidized bed gasifier.

2. MATERIALS AND METHODS

2.1. Feedstocks. Four biomasses, corn stalks (Cs), pine sawdust (Ps), Jerusalem artichoke stalks (JAs), and common reed (Re), were used in this work. Cs were collected from rural areas in Shandong Province, Ps from a Qingdao wood processing plant, and Re and JAs from coastal wetlands in the Yellow River Delta, China. All biomass samples' powder (particle size ≤ 180 μm) was used as received and stored in a desiccator until further analysis. The proximate analysis was carried out according to the Chinese GB/T 28731-2012 National Standards, and the ultimate analysis was measured by an Elementar Analysensysteme Gmbh (Vario MACRO cube, Germany).[30] The physicochemical characterizations of Cs, Ps, JAs, and Re are listed in Table 1. The Ps (87.76%) and Re (80.86%) have a higher amount than Cs (71.85%) and JAs (67.40%) in the content of volatile matter. The ash content is

Table 1. Feedstocks' Properties

(a) Proximate and Ultimate Analysis of Biomass Feedstocks				
Parameter	Cs	Ps	Re	JAs
Proximate analysis[a] (wt %, ad. Basis)				
Moisture	5.46	7.52	2.15	12.76
Ash	9.81	0.33	3.90	3.96
Volatile matter	69.85	84.76	77.97	77.25
Fix carbon[c]	14.88	7.39	5.98	6.03
Ultimate analysis[b] (wt %, daf. Basis)				
C	41.65	50.27	49.71	33.6
H	5.66	5.75	5.71	6.36
O[c]	36.33	32.10	36.97	42.79
N	0.95	2.52	1.16	0.53
S	0.14	0.00	0.40	0.00
HHV (MJ/kg)	16.61	20.62	19.32	18.28

(b) Chemical Composition Analysis				
Feedstock	Cellulose (wt %)	Hemicellulose (wt %)	Lignin (wt %)	Extractives (wt %)
Cs	65.25	8.65	0.00	26.10
Ps	57.21	13.98	25.45	3.36
JAs	63.63	16.56	7.44	12.37
Re	43.05	30.68	20.34	5.93

[a]Dry-free basis. [b]Dry ash-free basis. [c]Calculated by difference.

https://doi.org/10.1021/acsomega.1c06363
ACS Omega 2022, 7, 10144−10155

Table 2. Summary of Isoconversional Models for the Pyrolysis Kinetics in This Study

Model governing	Equation	Eq	Remarks	References
Friedman	$\ln\left(\beta\frac{d\alpha}{dT}\right) = \ln[Af(\alpha)] - \frac{E_a}{RT}$	(1)	The value of $\ln(\beta d\alpha/dT)$ was a function of $1/T$ at different heating rates; it is easy to obtain values of E_a at different conversions.	31
FWO	$\ln\beta = \ln\left(\frac{AE_a}{Rg(a)}\right) - 5.331 - \frac{1.052E_a}{RT}$	(2)	The activation energies can be obtained by plotting $\ln\beta$ vs $1/T$ at different heating rates when the conversion is a constant.	32, 33
KAS	$\ln\left[\frac{\beta}{T_2}\right] = \ln\frac{AR}{E_a g(a)} - \frac{E_a}{RT}$	(3)	$\ln\beta/T^2$ must have a good linear relationship with $1/T$ with $-(E_a/R)$ as the slope, which can calculate the activation energy.	34, 35

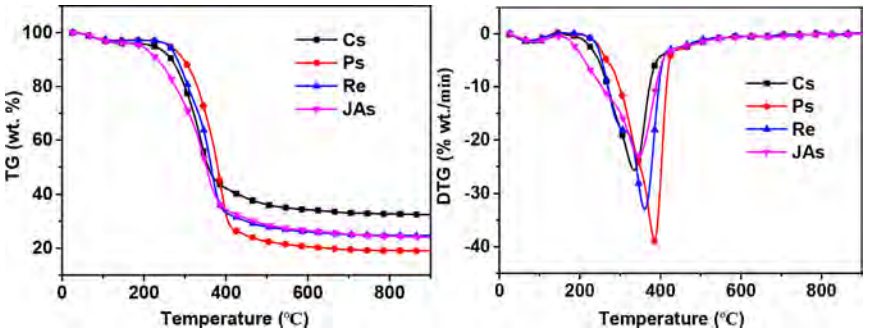

Figure 1. TG/DTG curve of typical biomass pyrolysis.

very high for Re (12.32%), followed by Cs (11.15%) and less in JAs (3.34%) and Ps (1.40%). The chemical analysis of biomass reveals that Cs, Ps, Re, and JAs are rich in cellulose content (43.05%−65.25%). Hemicellulose varied from 8.65% to 30.68%, while lignin varied from 0.00% to 25.45%.

2.2. Thermogravimetric Analysis. The pyrolysis measurements for the land and coastal zone species were conducted in thermal gravimetric analyzer (NETZSCH Instruments, STA 449 F3 Jupiter, Germany) in a continuous atmosphere of inert nitrogen (99.999 purity) at a flow rate of 100 mL/min to investigate the mass loss of biomass and the formation of volatiles. The operation process of TGA was based as per the reported method.[30] Six different heating rates were applied in this study: 50, 80, 100, 300, and 600 °C/min.

2.3. Kinetic Theory. *2.3.1. Isoconversional Methods.* Three isoconversional models (Friedman,[31] Flynn−Wall−Ozawa (FWO),[32,33] and Kissinger−Akahira−Sunose (KAS))[34,35] were selected to explain the kinetics of pyrolysis conversation. These models are summarized in Table 2.

2.3.2. DAEM. The DAEM $f(\alpha)$ reaction function often adopts the reaction series model, which can be described by eq 4.

$$1-\alpha = \begin{cases} \int_0^\infty \exp\left[-\int_{T_0}^{T}\frac{A}{\beta}\exp\left(-\frac{E}{RT}\right)dT\right]f(E)dE & n=1 \\ \int_0^\infty\left[1-(1-n)\int_{T_0}^{T}\frac{A}{\beta}\exp\left(-\frac{E}{RT}\right)dT\right]^{1/1-n} f(E)dE & n\neq 1 \end{cases} \quad (4)$$

The calculation methods of kinetic parameters can be divided into the distribution fitting method and the distribution-free method. The distribution fitting method achieves a highly accurate fitting by forcing the simulation of the TG data to obtain the parameters, but the calculation process is very complicated. The distribution-free method uses the equal transformation rate method to determine the correlation between E_a and α, and the calculation process is relatively simple. The Miura differential method and the Miura−Maki integration method[36] are common distribution-free methods, and the formula can be obtained by mathematical simplification:[36]

$$\ln\left(\frac{\beta}{T^2}\right) = \ln\left(\frac{AR}{E_a}\right) + 0.6075 - \frac{E_a}{R}\frac{1}{T} \quad (5)$$

2.4. Py-GC/MS Analysis. Pyrolysis product distributions of biomasses derived from land (Cs and Ps) and the coastal zone (Re and JAs) were carried out in a Py-GC/MS (CDS 5250, Agilent 7890B/5977A). The heating rate of the method was as high as 20000 °C/s, which can analyze the pyrolysis oil and gas online, avoiding the secondary reaction between volatiles and char in the traditional fast pyrolysis process effectively, which is closer to the tar composition obtained under the actual conditions. About 0.3 mg of samples was pyrolyzed at five different temperatures of 700, 750, 800, 850, and 900 °C for 20 s at 10000 °C/s. For the specific heating program of the Py-GC/MS, please refer to the literature.[21]

3. RESULTS AND DISCUSSION

3.1. Thermogravimetric Analysis. Figure 1 shows the TG/differential-thermogravimetric (DTG) curves of biomass pyrolysis at a heating rate of 50 °C/min. Table 3 lists the pyrolysis characteristics parameters (T_i, initial temperature; T_m, maximum degradation rate temperature; T_f, final temperature; R_{max}, maximum mass loss rate; m_f, residue quality). As expected, the biomass pyrolysis process is mainly divided into three stages: The first stage is the drying stage (<150 °C). The precipitation of free water mainly occurs in this stage, which shows a slight weight loss on the DTG curve. The second stage is the main pyrolysis stage (150−550 °C). In this stage, the biomass undergoes obvious thermal decomposition and volatiles are precipitated. The DTG curve shows an

https://doi.org/10.1021/acsomega.1c06363
ACS Omega 2022, 7, 10144−10155

Table 3. Pyrolysis Characteristic Parameters

Parameters	Cs	Ps	Re	JAs
T_i (°C)	252.6	268.9	260.4	187.0
T_1 (°C)			301.8	
T_m (°C)	339.0	387.2	336.0	362.8
R_1 (%/min)			−18.9	
R_{max} (%/min)	29.3	41.4	39.1	27.0
T_f (°C)	528.4	577.9	513.9	538.9
$\Delta T_{1/2}$ (°C)	74.2	72.8	48.8	82.7
D (10^{-6} % min^{-1} $°C^{-3}$)	4.6	5.5	9.2	4.8

obvious weight loss peak. For different biomasses, the DTG curves of Cs are relatively smooth, those of Ps and JAs are slightly curved, and and those of Re have obvious shoulder peaks. The obvious weight loss peak is mainly caused by the differences in the cellulose, hemicellulose, and lignin contents (Table 2). The third stage is the slow decomposition stage of the residue, in which the yield of the solid residue obtained by the pyrolysis of the biomass can be obtained.

The T_i values mainly reflect the thermal stabilities of different biomass samples. It can be seen from Table 3 that the order of the T_i values of four biomasses from small to large is JAs < Cs < Re < Ps, indicating that Ps has good thermal stability. The main component of JAs is inulin (monosaccharide). After heating, the thermal decomposition reaction occurs rapidly due to the low chemical bond energy. The R_m value of Ps is the largest, followed by Re, Cs, and JAs. The T_m value corresponds to R_m. The T_m values of Cs and Re are 339.0 and 336.0 °C respectively, while the T_m value of Ps is higher, 387.2 °C, which may be due to the inorganic mineral metal ions contained in ash as catalysts in the pyrolysis processes of Cs and Re.[37,38]

In order to comprehensively evaluate the difficulty of pyrolysis for various biomasses, an article proposed a comprehensive pyrolysis index D to reflect the pyrolysis characteristics of biomass.[39] The calculation method is as follows:

$$D = R_{max}/T_i T_m \Delta T_{1/2} \quad (6)$$

where D is the volatile emission index in % $°C^{-1}$ min^{-1} 10^{-8}, R_{max} is the maximum mass loss rate in % min^{-1}, T_i is the primary pyrolysis temperature in °C, T_m is the temperature corresponding to the maximum weight loss rate in °C, and ΔT is the half peak width of the maximum DTG peak in °C.

As shown in the table, the order of the D values from large to small is Re > PS > JAs > Cs. Therefore, the pyrolysis performances of Re and Ps are obviously better than those of Cs and JAs. In addition, it can be concluded that the order of the residual product yields from more to less is Cs > Re > JAs > Ps. Lignin is the main contribution component of solid residues in biomass pyrolysis. The content of the lignin component in Cs is high, and its ash content is high due to the influence of the growth environment, resulting in the high content of pyrolysis residue. The high content of Ps volatiles leads to less solid residue yield.

3.2. Effect of Heating Rate on Pyrolysis Behavior. The effect of heating rate (50, 80, 100, 300, and 600 °C/min) on biomass thermogravimetric characteristics is shown in Figure 2 and Table 4. With the increase of the heating rate, the decomposition rate of biomass accelerated, the TG/DTG curves of the samples all shifted to the high-temperature region, and the T_m value increased significantly. The mass loss of Cs at 50 °C/min in the main thermal cracking stage started at 254.9 °C and ended at 377.9 °C, during which 29.3%/min of the maximum mass loss rate occurred at 338.7 °C. However, T_i was 289.7 and 291.1 °C, and T_f was 385.7 and 428.0 °C for Cs at 300 °C/min and 600 °C/min, respectively. The T_i, T_f, and R_{max} corresponding to T_m were all increased as the heating rate increased. The response time of the temperature required for the pyrolysis of fuel particles is shortened with the increase of the heating rate, which promotes the progress of the pyrolysis process, resulting in an increase in T_i.[40] The increase in T_m, T_f, and R_{max} is mainly due to the thermal hysteresis effect.[41] With higher heating rate and larger temperature difference between the heater and samples due to the resistance of heat transfer, the thermal cracking was delayed.[40] Morover, the organic matter in the biomass is easily decomposed at high temperatures, so the values of R_{max} and D_i also increase. The D_i value increases with the increase of the heating rate, indicating that with the increase of the heating rate, the pyrolysis performance of the material is better, and the high heating rate is more conducive to the progress of the pyrolysis reaction. Further analysis shows that, taking Cs as an example, there is a good linear relationship between R_{max} and the heating rate at each heating rate, and the specific relationship is $y = 6.03 - 0.60x$ ($R^2 = 0.9985$).

The yield of the residue (char) was decreased with the heating rate increases. From this, we can conclude that higher heating rates deepen the thermal cracking process of biomass. In this stage, the hemicellulose in biomass continuously decomposed into char at a very slow rate from the temperature of 600 °C onward.[42] Moreover, other factors to consider are structural reordering with prolonged residence time, leading to a decreased intrinsic reactivity of the biomass.

From Figure 2, it can be seen that excluding the stage of removal of adsorbed water and low-molecular-weight hydrocarbons, land biomass has only one reactive stage in the pyrolysis process, while the coastal biomass presents two stages. As depicted in Table 1b, Cs has the highest content of cellulose (65.25 wt %), while Re has the least cellulose content (43.05 wt %). The hemicellulose content of Re is the highest (30.68 wt %) followed by JAs (16.56 wt %) and Ps (13.98 wt %); the least is Cs (8.65 wt %). Additionally, Ps (25.45 wt %) and Re (20.34 wt %) are abundant in the content of lignin. As reported in the previous literature, hemicellulose can be decomposed in the temperature range 220−315 °C.[43] Cellulose is a linear structure; it can be cracked in a higher temperature range (315−550 °C).[43] This coincides with the two reactive stages in Figure 2. Lignin generally degrades above 600 °C as it is full of heavily cross-linked aromatic rings.[44]

3.3. Kinetic Analysis. *3.3.1. Kinetic Parameters by Using Isoconversional Methods.* The E_a values calculated for all the isoconversional methods (Friedman, FWO, and KAS) were obtained by linear regression. Considering the complexity of four models and four biomass species, Figure S1 only shows the linear regressions constructed by using three different heating rates of 50, 80, and 100 °C/min to estimate the apparent activation energies for the Ps and JAs maxima using models. The variations of E_α (α is from 0.05 to 0.95) obtained from three different models for four biomass species are presented in Tables S1−S3, respectively.

The linear regression curve obtained by the four kinetic methods has its own characteristics. The linear regression straight line formed by the three points at different pyrolysis heating rates using the Friedman method exhibits a parabolic

https://doi.org/10.1021/acsomega.1c06363
ACS Omega 2022, 7, 10144−10155

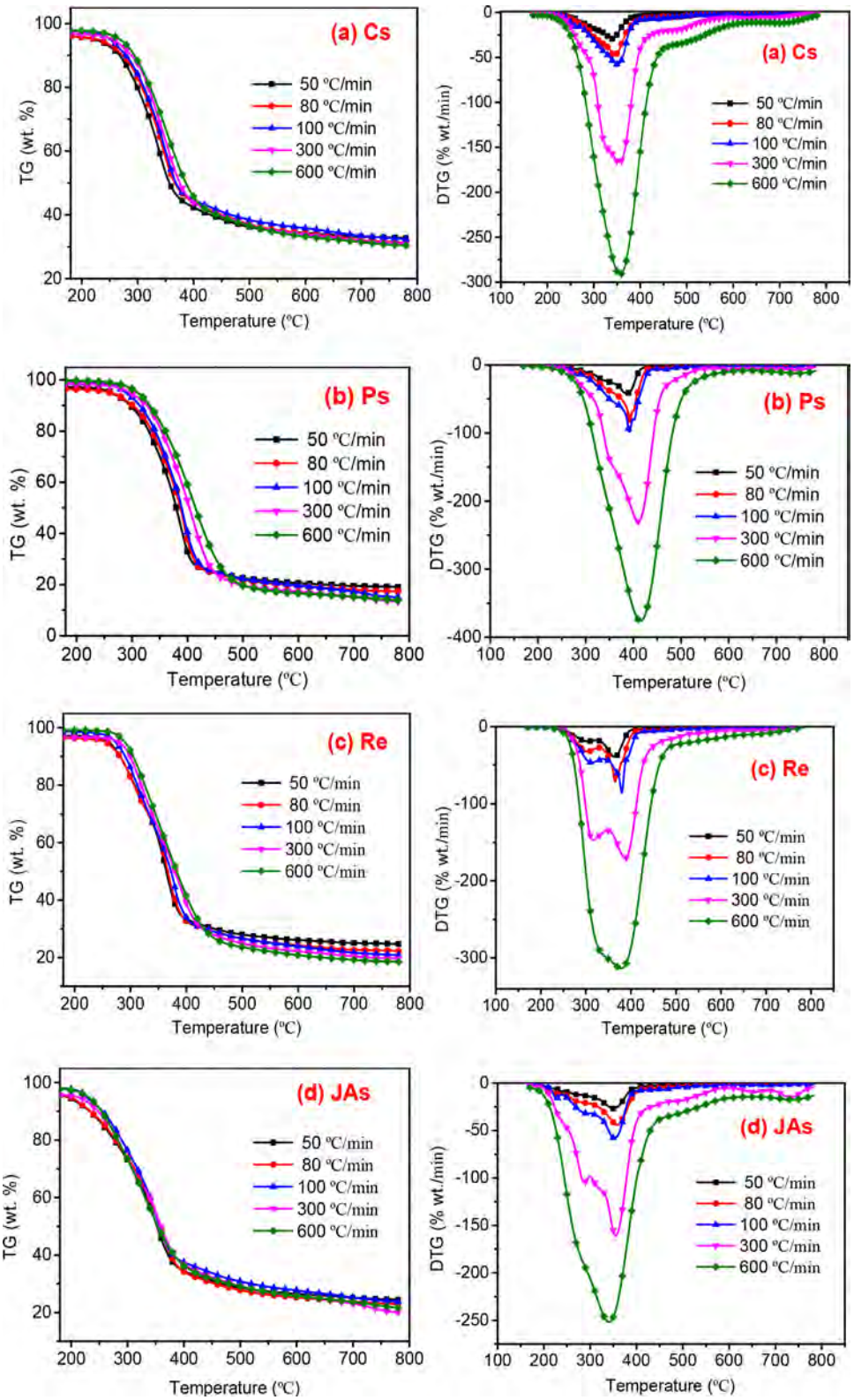

Figure 2. TG/DTG curves of biomass pyrolysis under different heating rates.

shape with the change of the pyrolysis temperature. The linear regression curve obtained by the FWO method is parallel to each other in the horizontal direction, while the curve fitted by the DAEM is a linear continuation of parallel lines in the tilting direction. This is mainly due to the difference in the integral equations of the three kinetic methods. Additionally, the Y-coordinate values at the same conversion rate under the same heating rate conditions calculated by the three kinetic methods also have significant differences, wherein the Friedman and FWO equations are positive and the latter is higher than the former.

https://doi.org/10.1021/acsomega.1c06363
ACS Omega 2022, 7, 10144−10155

Table 4. Pyrolysis Performance Index for Biomass at Different Heating Rates

	Parameters	Cs	Ps	Re	JAs
50 °C/min	T_i (°C)	254.9	304.1	178.2	255.7
	T_1 (°C)			302.1	
	T_m (°C)	338.7	385.3	363.8	350.6
	R_1 (%/min)			18.92	
	R_{max} (%/min)	29.3	38.9	39.0	25.9
	T_f (°C)	377.9	420.5	395.6	397.0
	$\Delta T_{1/2}$ (°C)	67.2	77.0	49.0	94.0
	D (10^{-6} % min^{-1} $°C^{-3}$)	5.0	4.3	12.3	2.9
	m_f (%)	32.7	19.3	25.1	24.2
80 °C/min	T_i (°C)	264.2	375.1	260.4	247.3
	T_1 (°C)			301.3	
	T_m (°C)	337.7	392.7	364.8	358.2
	R_1 (%/min)			32.10	
	R_{max} (%/min)	41.0	84.2	71.8	44.2
	T_f (°C)	396.9	421.5	387.6	401.8
	$\Delta T_{1/2}$ (°C)	81.6	48.0	40.0	78.0
	D (10^{6} % min^{-1} $°C^{-3}$)	6.0	11.9	18.9	5.5
	m_f (%)	30.5	16.7	25.0	23.3
100 °C/min	T_i (°C)	275.0	374.2	261.3	248.0
	T_1 (°C)			174.0	
	T_m (°C)	344.7	391.9	375.1	362.8
	R_1 (%/min)			0.43	
	R_{max} (%/min)	52.6	98.4	77.3	54.0
	T_f (°C)	395.2	427.0	409.8	409.8
	$\Delta T_{1/2}$ (°C)	79.5	62.0	59.0	87.0
	D (10^{6} % min^{-1} $°C^{-3}$)	7.9	10.8	13.4	5.9
	m_f (%)	29.9	13.9	21.6	23.3
300 °C/min	T_i (°C)	289.7	310.2	278.0	232.1
	T_1 (°C)			316.6	
	T_m (°C)	354.9	410.3	386.7	350.3
	R_1 (%/min)			146.78	
	R_{max} (%/min)	166.7	229.6	170.6	149.3
	T_f (°C)	385.7	458.8	432.5	401.9
	$\Delta T_{1/2}$ (°C)	79.5	98.0	120.0	110.0
	D (10^{6} % min^{-1} $°C^{-3}$)	20.30	18.41	13.22	16.69
	m_f (%)	29.9	13.3	18.6	22.0
600 °C/min	T_i (°C)	291.1	278.6	269.0	223.9
	T_1 (°C)				
	T_m (°C)	355.9	415.2	378.3	356.5
	R_1 (%/min)				
	R_{max} (%/min)	291.3	376.0	313.5	269.0
	T_f (°C)	428.0	495.2	459.6	428.8
	$\Delta T_{1/2}$ (°C)	105.9	122.0	137.0	142.0
	D (10^{6} % min^{-1} $°C^{-3}$)	30.3	26.6	22.5	23.7
	m_f (%)	29.6	12.6	18.1	21.2

Figure 3 shows the E_α distribution against α of substances for the Friedman (FR), FWO, and KAS methods. As observed, the E_α profiles of both land and coastal biomasses for the KAS and FWO methods are practically the same, while the E_α profile calculated by the Friedman method is slightly different. This is mainly due to the difference in the mathematical processing methods; the KAS and FWO methods are based on the integral form, while the FR method is based on the differential form.[7,11]

In relation to the variation of E_α obtained for the four samples, with the increase of α, E_α shows an overall upward trend, but there are fluctuations locally. This means that the chemical reactions involved in the pyrolysis process are complex, including a series of parallel, overlapping, and sequential reactions. As can be seen in Figure 5, E_α increases first and then decreases slightly, finally increasing significantly with the increase of α ($0.05 < \alpha < 0.95$) for the Cs, Ps, and Re species. However, for JAs, the E_α versus α relationship curve presents a W shape. The variation in E_α reflects the change in the strength of chemical bonds undergoing thermal cracking.[45] As the pyrolysis reaction proceeds, the stronger the chemical bond of the components, the more difficult it is to crack, and higher temperatures are needed to further pyrolyze the material. This corresponds to the decomposition of hemicellulose, cellulose, and lignin in section 3.2.[46] In the initial stages, the activation energy increases as the most unstable bonds are severed first. As the reaction proceeds, more stable bonds remain; thus, more energy is required to decompose the

https://doi.org/10.1021/acsomega.1c06363
ACS Omega 2022, 7, 10144−10155

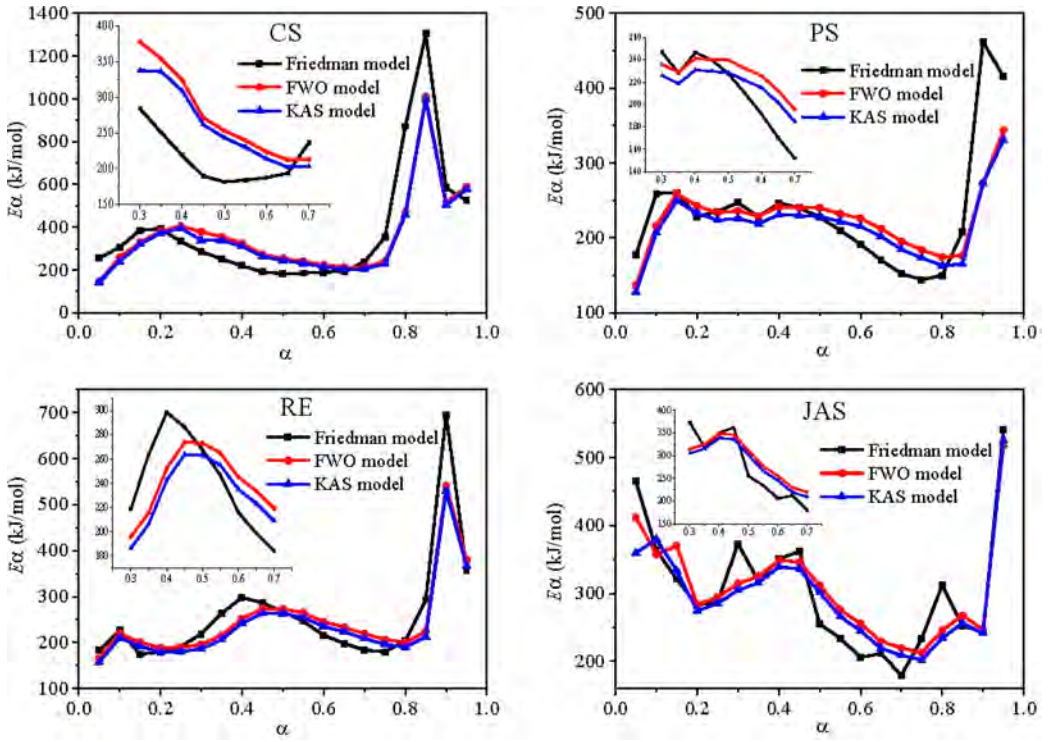

Figure 3. E_α versus α relationship estimated for land and coastal biomasses: Cs, corn stalks; Ps, pine sawdust; JAs, Jerusalem artichoke stalks; Re, reed.

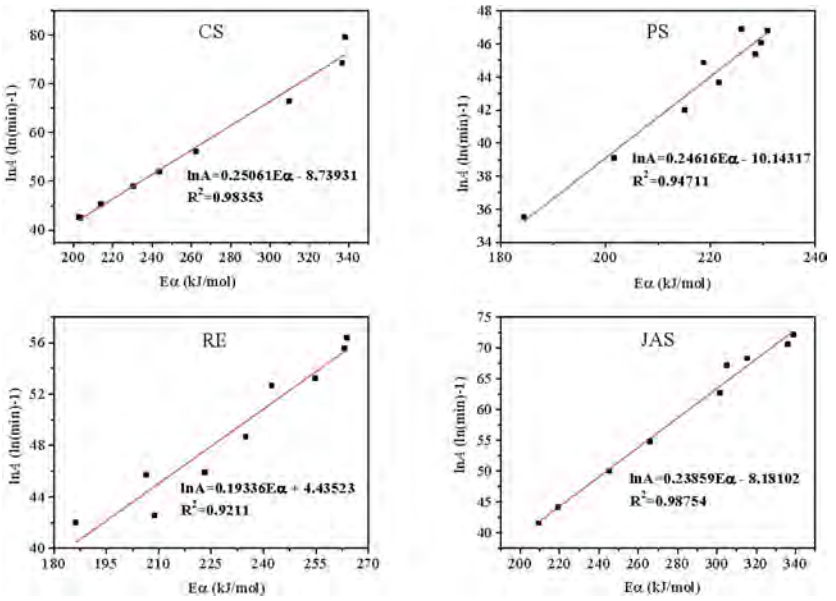

Figure 4. ln A versus E_α relationship estimated for land and coastal biomasses: JAs, Jerusalem artichoke stalks; Re, reed; Cs, corn stalks; Ps, pine sawdust.

biomass structure. Once enough energy is available to sever the more stable bonds in the biomass structure, radicals are formed. These radicals require less energy to further decompose, which is reflected in the decrease in activation energy. Then finally, as the radical species have decomposed to light gases and have been depleted, the only bonds left to cleave are the more stable bonds of the aromatic lignin. This is supported by the sharp increase in activation energy in the late stages of the reaction. Therefore, we often take the main thermal cracking stage ($30\% < \alpha < 70\%$) to conduct in-depth research. It can be seen in Figure 4, in the main thermal cracking stage, for Cs, that E_α gradually decreases from 377.80 and 338 kJ/mol to 212.67 and 202.71 kJ/mol between 30% and 65% conversion and then remains around 213 and 203 kJ/mol in the FWO and KAS methods, respectively. But, if we applied the Friedman method, E_α gradually decreases from 284.61 to 181.86 kJ/mol between 30% and 50% conversion and then increases to 236.95 kJ/mol between 50% and 70% conversion. Ps and JAs also present this trend. However, for Re, a different trend is observed. All three model methods

https://doi.org/10.1021/acsomega.1c06363
ACS Omega 2022, 7, 10144−10155

Table 5. Kinetic Parameters Obtained from the Distributed Activation Model (DAEM) for Cs, Ps, Re, and JAs[a]

	Cs			Ps			Re			JAs		
α	E_α (kJ/mol)	A (min^{-1})	R^2	E_α	A	R^2	E_α	A	R^2	E_α	A	R^2
0.10	198.4	6.87×10^{18}	0.995	196.3	1.27×10^{19}	0.996	145.9	2.40×10^{15}	0.986	322.5	1.09×10^{35}	0.928
0.20	230.5	1.08×10^{21}	0.953	225.5	8.38×10^{20}	0.967	171.9	2.55×10^{17}	0.998	274.8	2.20×10^{27}	0.981
0.30	236.0	9.64×10^{20}	0.935	233.7	1.09×10^{21}	0.948	202.0	5.61×10^{19}	0.966	306.6	2.21×10^{29}	0.987
0.40	239.7	7.03×10^{20}	0.956	236.5	6.23×10^{20}	0.951	264.6	8.41×10^{24}	0.928	338.9	2.28×10^{31}	0.992
0.50	232.3	6.82×10^{19}	0.995	241.3	5.93×10^{20}	0.976	276.4	1.78×10^{26}	0.914	301.4	1.64×10^{27}	0.999
0.60	207.5	2.84×10^{17}	0.996	223.7	8.89×10^{18}	1.000	289.3	9.37×10^{23}	0.917	245.4	5.25×10^{21}	0.999
0.70	177.3	4.93×10^{14}	0.981	188.4	5.52×10^{15}	0.992	264.1	1.71×10^{20}	0.940	209.2	1.17×10^{18}	0.997
0.80	167.0	3.12×10^{13}	0.949	165.9	4.09×10^{13}	0.974	254.2	3.26×10^{17}	0.924	234.4	1.17×10^{19}	0.998

[a]Cs, corn stalks; Ps, pine sawdust; JAs, Jerusalem artichoke stalks; Re, reed.

Table 6. Mean Values of Kinetic Parameters for Land and Coastal Biomasses in the Main Thermal Cracking Stage[a]

	Friedman		FWO		KAS		DAEM		
Samples	E_a	R^2	E_a	R^2	E_a	R^2	E_a	A	R^2
Cs	214.38	0.9957	274.72	0.9755	260.08	0.9934	211.09	3.53×10^{20}	0.977
Ps	212.48	09971	227.98	0.9948	217.39	0.9999	213.91	3.96×10^{20}	0.975
Re	242.14	0.9929	241.35	0.9915	231.50	0.9946	233.55	2.34×10^{25}	0.947
JAs	276.67	0.9976	291.38	0.9803	281.84	0.9928	279.15	1.36×10^{34}	0.985

[a]E_α (kJ/mol). A (min^{-1}). Cs, corn stalks; Ps, pine sawdust; JAs, Jerusalem artichoke stalks; Re: reed.

show a trend of increasing first and then decreasing between 30% and 70% conversion. They are just different in the dividing point. The dividing points of the conversion rates for the Friedman, FWO, and KAS models are 0.40, 0.45, and 0.45, respectively. Additionally, it is also believed that variations in the activation energy reflect a transformation in the nature of the rate-controlling step.[47]

3.3.2. Kinetic Parameters by Using the DAEM. The kinetic parameters obtained from the DAEM for Cs, Ps, Re, and JAs are shown in Table 5. It is observed that the plots are nonlinear and the conversions of different feedstocks show different behaviors. R^2 varies between 0.91 and 0.99 (>0.9) with the value of α ranging from 0.1 to 0.8, which implies the fitting effect of the linear fitting curve of the DAEM is better. The pyrolysis activation energy of Cs is between 167.0 and 239.7 kJ/mol, that of Ps is between 196.3 and 241.3 kJ/mol, that of Re is between 145.9 and 289.3 kJ/mol, and that of JAs is between 209.2 and 338.9 kJ/mol. The activation energies of different feedstocks show different trends with the increase of conversion, which was the same as the isoconversional methods. This shows that these biomasses have experienced a very complex degradation process related to different types of reactions. The frequency factor (A) calculated from the DEAM varies from 3.12×10^{13} to 1.08×10^{21} min^{-1} for Cs, 4.09×10^{13} to 1.09×10^{21} min^{-1} for Ps, 2.40×10^{13} to 1.78×10^{26} min^{-1} for Re, and 1.17×10^{18} to 1.09×10^{35} min^{-1} for JAs.

The mean values of E_α of the coastal and land biomasses calculated by the isoconversional method and the DAEM in the main stage are listed in Table 6. As observed, the mean values of E_α calculated using the Friedman, FWO, and KAS models are 214.38, 274.72, and 260.08 kJ/mol for Cs, 212.48, 227.98, and 217.39 kJ/mol for Ps, 242.14, 241.35, and 231.50 kJ/mol for Re, and 276.67, 291.83, and 281.84 for JAs. These values are close to those reported in the aforementioned literature.[10,48] JAs have the largest E_α value during the pyrolysis process, followed by Cs, and Ps and Re show similar activation energies. This indicates that the mean value of the chemical bond energy in the JAs' structure is the largest, while the chemical bond energies of Ps and Re are weaker. Compared with the other three biomasses, JAs show the highest E_a value by the DAEM and the isoconversional method. This indicates that when designing the pyrolysis system, higher energy is required to process JAs completely. In relation to the activation energies calculated by the different models, since the Friedman method considers both the heating rate and the raw data and it is related to the simple differential form of the kinetic rate law and does not contain an overly simplified approximation, the KAS and OFW models and the DAEM are conversional dependent models; therefore, the Friedman model predicts comparably accurate kinetic data compared with the DAEM.

3.3.3. Kinetic Compensation Effect. The ln A versus E_α relationship estimated for land and coastal biomasses in the main thermal cracking stage are shown in Figure 4. As can be seen, Cs and JAs have a good linear relationship between ln A and E_α during the main pyrolysis stage, while PS and Re are relatively weaker. In the stage of the reaction conversion rate at 30−50%, the ln A and E_α of Cs and JAs have a highly linear relationship, while the linear relationship of Re is weak, and the regression coefficient is only 0.92. The linear compensation relationship between ln A and E_α is called the kinetic compensation effect.[49]

The linear compensation relationship between ln A and E_α does not necessarily indicate the existence of a kinetic compensation effect due to the influence of systematic error propagation and mass transfer caused by sample temperature deviation during the experiment.[49] However, biomass samples are placed on the top of the thermocouple (STA449F3) to ensure the accuracy of weight loss and recorded temperatures. Moreover, the mass of the sample is controlled within 5 mg during the experiment, and the smaller sample quality ensures the minimization of the mass transfer effect during the reaction. Therefore, both land and coastal biomasses have different degrees of kinetic compensation effect in different pyrolysis processes, and the degree of compensation effect varies depending on the composition of each biomass sample. In the pyrolysis of complex multicomponent organic matter such as biomass, the thermal decomposition reaction becomes more difficult as the reaction progresses, showing higher E_α

https://doi.org/10.1021/acsomega.1c06363
ACS Omega 2022, 7, 10144−10155

and A values. It is somewhat unclear as to why the increase in activation energy is offset by the increase in frequency factor for Cs and JAs but not for Ps and Re.

3.4. High-Temperature Fast Pyrolysis Product Analysis. *3.4.1. Effect of Feedstock Properties.* Figure 5 depicts

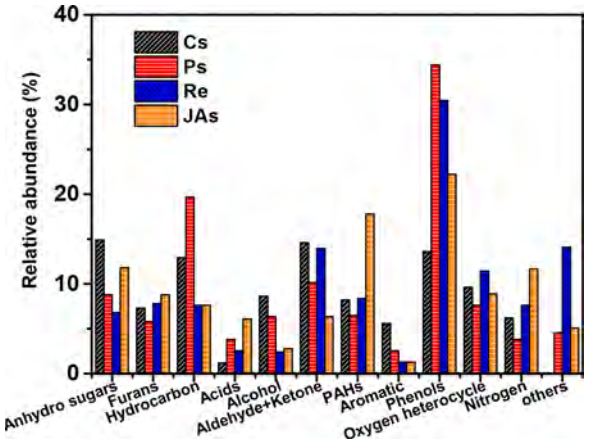

Figure 5. Product distribution from high-temperature fast pyrolysis of different biomasses. JAs, Jerusalem artichoke stalks; Re, reed; Cs, corn stalks; Ps, pine sawdust.

the major class of compounds obtained from fast pyrolysis of the four different kinds of biomass at 800 °C for 20 s at 10000 °C/s. The compounds were classified into the following categories: anhydro sugars, furans, hydrocarbons, aldehydes + ketones, acids, alcohols, polycyclic aromatic hydrocarbons (PAHs), phenols, aromatics, oxygen heterocycles, nitrogen compounds, and others. The organics were quantified by their peak area% values. It can be seen that the fast pyrolysis of biomass under high temperature resulted in phenols, hydrocarbons, PAHs, and oxygen heterocycle compounds, followed by anhydro sugars, aldehydes + ketones, and furans but fewer acids and aromatics. Comparing the products of four kinds of biomass, it can be seen that the order of phenols' yields from more to less is Ps > Re > JAs > Sp. It can be seen from the foregoing that the main components of the four biomasses are cellulose, hemicellulose, and lignin, and each compound of the pyrolysis product species can be related to the pyrolysis of the above components. The formation of phenol compounds is mainly derived from the thermal cracking of lignin. Since Ps has a higher proportion of lignin components, the selectivity of phenols in its pyrolysis products is higher. The small amount of phenols in Cs originates from the cracking of the protein component.[50] Anhydro sugars and aldehyde + ketone compounds are the major products, respectively, from the fast pyrolysis of Cs at high temperature. This is mainly due to its rich cellulose and hemicellulose components. The content of anhydro sugars, PAHs, and acids in JAs is relatively high, which is mainly related to its main components. JAs contain a large amount of inulin, and the inulin molecule consists of about 31 β-D-fructose moieties and 1−2 linear polysaccharides formed by the polymerization of inulin residues. Linear polysaccharides undergo decarboxylation and decarbonylation reactions at high temperature, and molecular bonds are broken

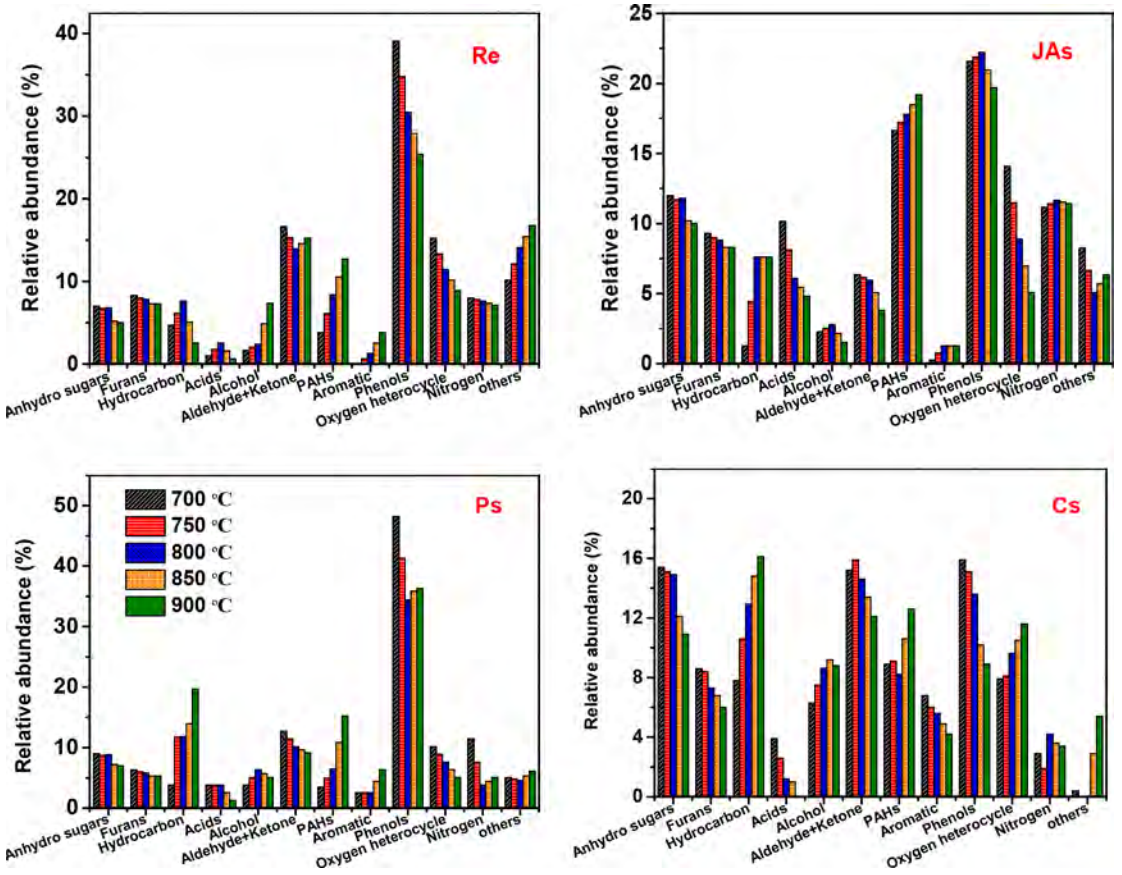

Figure 6. Fast pyrolysis products of different biomasses under different temperature conditions.

https://doi.org/10.1021/acsomega.1c06363
ACS Omega 2022, 7, 10144−10155

and recombined to generate PAHs with better thermal stability.[40]

3.4.2. Effect of Temperature. The selectivity of each group of biomass fast pyrolysis products at different temperatures is shown in Figure 6. It can be seen that the pyrolysis temperature has a great influence on the selectivity of each group of products. At 700 °C, the selectivities of anhydro sugars, furans, aldehydes + ketones, phenols, oxygenated heterocycles, and nitrogen compounds in Re waste are 7.0%, 8.3%, 16.6%, 39.1%, 15.2%, and 7.9%, respectively. As the temperature increases to 900 °C, the above categories are reduced to 5.2%, 7.3%, 15.2%, 25.4%, 8.9%, and 7.1%, respectively. The selectivities of PAHs and aromatic compounds increase from 3.8% and 0.2% to 12.7% and 3.8%, respectively. The selectivities of hydrocarbons, acids, and alcohols increased first and then decreased.

Hydrocarbons mainly include hydrocarbons and aromatic hydrocarbons. At high temperature, light hydrocarbon products mainly come from the deep cracking reaction of aldehydes, ketones, acids, and other compounds, while aromatic hydrocarbon products are mainly generated in two ways: one is derived from the dehydroxylation and decarbonylation of phenolic compounds; the other is derived from the polymerization, cyclization, and dehydrogenation of light hydrocarbon products. With the increase of temperature from 700 to 900 °C, the selectivity of PAHs increases rapidly. PAHs are highly toxic carcinogens, mainly from the polycondensation of tar components. When the temperature reaches 700 °C, a large number of oxygenated and substituent-containing aromatic compounds begin to transform, and the tar component gradually removes the substituents on the aromatic ring to form a more stable aromatic or five-carbon-ring-containing phenolic group or methyl group. With the increase of temperature, the five-carbon ring generates unsaturated double and triple bonds through addition and cleavage. The resulting double bond and triple bond products are gradually cyclized by an acetylene addition reaction, etc., and the aromatic hydrocarbons are further dehydrocyclized and converted into polycyclic aromatic hydrocarbons or carbon black with a higher degree of polymerization.

The main components of oxygenated compounds in the rapid pyrolysis products of biomass at high temperature are phenols, while the selectivities of other oxygenated compounds, including anhydro sugars, furans, acids, aldehydes, and ketones, decrease with the increase of temperature. This is mainly attributed to the main chemical bonds of oxygen-containing compounds being C−O, C−H, and C−C bonds, of which the C−O bond is weaker, followed by the C−H bond, and the C−C bond having the strongest bond energy. The increase of temperature leads to the first fracture of the C−O bond; decarboxylation, decarbonylation, dehydrogenation, and aromatization reactions occur respectively, resulting in the conversion of oxygenated compounds into more stable phenolic and aromatic compounds at high temperature.

4. CONCLUSIONS

A series of thermogravimetric experiments under the heating rate from 50 °C/min to 600 °C/min was conducted to compare the pyrolysis behaviors of typical land (Cs and Ps) and coastal zone (Re and JAs) biomasses. The D_i value increases with the increase of the heating rate, indicating that high heating rate is more conducive to the progress of the pyrolysis reaction. There is a good linear relationship between R_{max} and the heating rate at each heating rate. The initial decomposition temperature for coastal biomasses (Re and JAs) was lower compared to land biomasses (Cs and Re). JAs has the largest E_α value during the pyrolysis process, followed by Cs. The activation energy values of Ps and Re are relatively close. The DAEM showed that Cs and JAs have a good linear relationship between ln A and E_α during the main pyrolysis stage, while Ps and Re are relatively weaker. The kinetic compensation effect was evident for Cs and JAs during the main thermal cracking stage. In addition, the Py-GC/MS results exhibited that phenols, hydrocarbons, PAHs, and oxygen heterocycle compounds were strongly present in the obtained volatile compounds. Also, some oxygen-containing volatiles are easily converted into aromatic products with higher stability under high temperature. High-temperature fast pyrolysis of JAs produced a larger amount of PAHs compounds whereas larger amounts of hydrocarbons and phenols were generated from pyrolysis of Ps.

■ ASSOCIATED CONTENT

Supporting Information

The Supporting Information is available free of charge at https://pubs.acs.org/doi/10.1021/acsomega.1c06363.

Results of E_α based on the FWO, KAS, and Friedman method; kinetic plots of the isoconversional and DAEM methods (PDF)

■ AUTHOR INFORMATION

Corresponding Author

Zhengyi Liu − *Yantai Institute of Coastal Zone Research, Chinese Academy of Sciences, Yantai, Shandong 264003, China*; Email: zyliu@yic.ac.cn

Authors

Jie Li − *College of Safety and Environmental Engineering, Shandong University of Science and Technology, Qingdao, Shandong 266590, China*; orcid.org/0000-0002-0048-4637

Yanchao Shang − *State Key Laboratory of Heavy Oil Processing, China University of Petroleum (East China), Qingdao, Shandong 266580, China*

Wei Wei − *State Key Laboratory of Heavy Oil Processing, China University of Petroleum (East China), Qingdao, Shandong 266580, China*

Yingyun Qiao − *State Key Laboratory of Heavy Oil Processing, China University of Petroleum (East China), Qingdao, Shandong 266580, China*

Song Qin − *Yantai Institute of Coastal Zone Research, Chinese Academy of Sciences, Yantai, Shandong 264003, China*

Yuanyu Tian − *State Key Laboratory of Heavy Oil Processing, China University of Petroleum (East China), Qingdao, Shandong 266580, China*; orcid.org/0000-0003-3326-7484

Complete contact information is available at: https://pubs.acs.org/10.1021/acsomega.1c06363

Author Contributions

‖Y.S. contributed to the work equally and should be regarded as co-first author.

Notes

The authors declare no competing financial interest.

https://doi.org/10.1021/acsomega.1c06363
ACS Omega 2022, 7, 10144−10155

■ ACKNOWLEDGMENTS

This work was supported by the Taishan Scholar Foundation of Shandong Province (Grant number: tsqn201812028) and the Department of Science and Technology of Shanxi Province (Grant number: 2020ZDLSF06-10).

■ REFERENCES

(1) Yuan, Y.; Duan, H.; Tsvetanov, T. G. Synergizing China's energy and carbon mitigation goals: General equilibrium modeling and policy assessment. *Energy Econ* **2020**, *89*, 104787.
(2) Kant Bhatia, S.; Palai, A. K.; Kumar, A.; Kant Bhatia, R.; Kumar Patel, A.; Kumar Thakur, V.; Yang, Y.-H. Trends in renewable energy production employing biomass-based biochar. *Bioresour. Technol.* **2021**, *340*, 125644.
(3) Yang, Q.; Zhou, H.; Bartocci, P.; Fantozzi, F.; Mašek, O.; Agblevor, F. A.; Wei, Z.; Yang, H.; Chen, H.; Lu, X.; Chen, G.; Zheng, C.; Nielsen, C. P.; McElroy, M. B. Prospective contributions of biomass pyrolysis to China's 2050 carbon reduction and renewable energy goals. *Nat. Commun.* **2021**, *12* (1), 1698.
(4) Maduskar, S.; Maliekkal, V.; Neurock, M.; Dauenhauer, P. J. On the Yield of Levoglucosan from Cellulose Pyrolysis. *ACS Sustain. Chem. Eng.* **2018**, *6* (5), 7017−7025.
(5) Tomczyk, A.; Sokołowska, Z.; Boguta, P. Biochar physicochemical properties: pyrolysis temperature and feedstock kind effects. *Rev. Environ. Sci. Biotechnol* **2020**, *19* (1), 191−215.
(6) Tao, W.; Yang, X.; Li, Y.; Zhu, R.; Si, X.; Pan, B.; Xing, B. Components and Persistent Free Radicals in the Volatiles during Pyrolysis of Lignocellulose Biomass. *Environ. Sci. Technol.* **2020**, *54* (20), 13274−13281.
(7) Arenas, C. N.; Navarro, M. V.; Martínez, J. D. Pyrolysis kinetics of biomass wastes using isoconversional methods and the distributed activation energy model. *Bioresour. Technol.* **2019**, *288*, 121485.
(8) Burra, K. R. G.; Gupta, A. K. Modeling of biomass pyrolysis kinetics using sequential multi-step reaction model. *Fuel* **2019**, *237*, 1057−1067.
(9) Luo, L.; Guo, X.; Zhang, Z.; Chai, M.; Rahman, M. M.; Zhang, X.; Cai, J. Insight into Pyrolysis Kinetics of Lignocellulosic Biomass: Isoconversional Kinetic Analysis by the Modified Friedman Method. *Energy Fuels* **2020**, *34* (4), 4874−4881.
(10) Mishra, R. K.; Mohanty, K. Pyrolysis kinetics and thermal behavior of waste sawdust biomass using thermogravimetric analysis. *Bioresour. Technol.* **2018**, *251*, 63−74.
(11) Cai, J.; Xu, D.; Dong, Z.; Yu, X.; Yang, Y.; Banks, S. W.; Bridgwater, A. V. Processing thermogravimetric analysis data for isoconversional kinetic analysis of lignocellulosic biomass pyrolysis: Case study of corn stalk. *Renew. Sust. Energy Rev.* **2018**, *82*, 2705−2715.
(12) He, Q.; Ding, L.; Gong, Y.; Li, W.; Wei, J.; Yu, G. Effect of torrefaction on pinewood pyrolysis kinetics and thermal behavior using thermogravimetric analysis. *Bioresour. Technol.* **2019**, *280*, 104−111.
(13) Hameed, S.; Sharma, A.; Pareek, V.; Wu, H.; Yu, Y. A review on biomass pyrolysis models: Kinetic, network and mechanistic models. *Biomass Bioenergy* **2019**, *123*, 104−122.
(14) Tahir, M. H.; Zhao, Z.; Ren, J.; Rasool, T.; Naqvi, S. R. Thermo-kinetics and gaseous product analysis of banana peel pyrolysis for its bioenergy potential. *Biomass Bioenergy* **2019**, *122*, 193−201.
(15) He, C.; Tang, C.; Liu, W.; Dai, L.; Qiu, R. Co-pyrolysis of sewage sludge and hydrochar with coals: Pyrolytic behaviors and kinetics analysis using TG-FTIR and a discrete distributed activation energy model. *Energy Convers. Manag* **2020**, *203*, 112226.
(16) Konwar, K.; Nath, H. P.; Bhuyan, N.; Saikia, B. K.; Borah, R. C.; Kalita, A. C.; Saikia, N. Effect of biomass addition on the devolatilization kinetics, mechanisms and thermodynamics of a northeast Indian low rank sub-bituminous coal. *Fuel* **2019**, *256*, 115926.
(17) Wang, S.; Dai, G.; Yang, H.; Luo, Z. Lignocellulosic biomass pyrolysis mechanism: A state-of-the-art review. *Prog. Energy Combust. Sci.* **2017**, *62*, 33−86.
(18) Cai, J.; Wu, W.; Liu, R. An overview of distributed activation energy model and its application in the pyrolysis of lignocellulosic biomass. *Renew. Sust. Energy Rev.* **2014**, *36*, 236−246.
(19) Várhegyi, G.; Szabó, P.; Antal, M. J. Kinetics of Charcoal Devolatilization. *Energy Fuels* **2002**, *16* (3), 724−731.
(20) Efika, C. E.; Onwudili, J. A.; Williams, P. T. Influence of heating rates on the products of high-temperature pyrolysis of waste wood pellets and biomass model compounds. *Waste Manage* **2018**, *76*, 497−506.
(21) Mishra, R. K.; Mohanty, K.; Wang, X. Pyrolysis kinetic behavior and Py-GC−MS analysis of waste dahlia flowers into renewable fuel and value-added chemicals. *Fuel* **2020**, *260*, 116338.
(22) Hidayat, S.; Abu Bakar, M. S.; Yang, Y.; Phusunti, N.; Bridgwater, A. V. Characterisation and Py-GC/MS analysis of Imperata Cylindrica as potential biomass for bio-oil production in Brunei Darussalam. *J. Anal Appl. Pyrolysis* **2018**, *134*, 510−519.
(23) Lu, Q.; Yang, X.-c.; Dong, C.-q.; Zhang, Z.-f.; Zhang, X.-m.; Zhu, X.-f. Influence of pyrolysis temperature and time on the cellulose fast pyrolysis products: Analytical Py-GC/MS study. *J. Anal Appl. Pyrolysis* **2011**, *92* (2), 430−438.
(24) Chen, W.-H.; Wang, C.-W.; Kumar, G.; Rousset, P.; Hsieh, T.-H. Effect of torrefaction pretreatment on the pyrolysis of rubber wood sawdust analyzed by Py-GC/MS. *Bioresour. Technol.* **2018**, *259*, 469−473.
(25) Ramesh, R.; Chen, Z.; Cummins, V.; Day, J.; D'Elia, C.; Dennison, B.; Forbes, D. L.; Glaeser, B.; Glaser, M.; Glavovic, B.; Kremer, H.; Lange, M.; Larsen, J. N.; Le Tissier, M.; Newton, A.; Pelling, M.; Purvaja, R.; Wolanski, E. Land−Ocean Interactions in the Coastal Zone: Past, present & future. *Anthropocene* **2015**, *12*, 85−98.
(26) Paul, D.; Lade, H. Plant-growth-promoting rhizobacteria to improve crop growth in saline soils: a review. *Agron Sustain Dev* **2014**, *34* (4), 737−752.
(27) Khajavi-Shojaei, S.; Moezzi, A.; Norouzi Masir, M.; Taghavi, M. Characteristics of conocarpus wastes and common reed biochars as a predictor of potential environmental and agronomic applications. *Energ Source Part A* **2020**, 1−18.
(28) Van Tran, G.; Unpaprom, Y.; Ramaraj, R. Methane productivity evaluation of an invasive wetland plant, common reed. *Biomass Convers. Biorefin* **2020**, *10* (3), 689−695.
(29) Bangqin, A. C. X. A. S. L. G. C. X. Z. J. S. The Economic Salttolerant Plant Resources on the Coastal Zone of China. *J. Nanjing Forestry University* **1999**, *42* (04), 81−84.
(30) Li, J.; Qiao, Y.; Zong, P.; Qin, S.; Wang, C.; Tian, Y. Fast pyrolysis characteristics of two typical coastal zone biomass fuels by thermal gravimetric analyzer and down tube reactor. *Bioresour. Technol.* **2019**, *283*, 96−105.
(31) Friedman, H. L. Kinetics of thermal degradation of char-forming platics from thermogravimetry. Application to a phenolic plastic. *J. Polym. Sci. Part C: Polym. Sym* **1964**, *6*, 183−195.
(32) Flynn, J. H.; Wall, L. A. A quick, direct method for the determination of activation energy from thermogravimetric data. *J. Polym. Sci. Part B: Polym. Lett.* **1966**, *4*, 323−328.
(33) Ozawa, T. A new method of analyzing thermogravimetric data. *Bull. Chem. Soc. Jpn.* **1965**, *38*, 1881−1886.
(34) Kissinger, H. E. Variation of peak temperature with heating rate in differential thermal analysis. *J. Res. Natl. Bur. Stand* **1956**, *57*, 217−221.
(35) Akahira, T. Joint convention of four electrical institutes. *Sci. Technol.* **1971**, *16*, 22−31.
(36) Miura, K.; Maki, T. A Simple Method for Estimating f(E) and k0(E) in the Distributed Activation Energy Model. *Energy Fuels* **1998**, *12* (5), 864−869.
(37) Lu, Y.; Wang, Y.; Wang, Q.; Zhang, J.; Zhao, Y.; Zhang, Y. Investigation on the catalytic effect of AAEMs on the pyrolysis characteristics of Changji oil shale and its kinetics. *Fuel* **2020**, *267*, 117287.

https://doi.org/10.1021/acsomega.1c06363
ACS Omega 2022, 7, 10144−10155

(38) Xiong, Z.; Guo, J.; Han, H.; Xu, J.; Jiang, L.; Su, S.; Hu, S.; Wang, Y.; Xiang, J. Effects of AAEMs on formation of heavy components in bio-oil during pyrolysis at various temperatures and heating rates. *Fuel Process. Technol.* **2021**, *213*, 106690.
(39) Wu, Z.; Wang, S.; Zhao, J.; Chen, L.; Meng, H. Synergistic effect on thermal behavior during co-pyrolysis of lignocellulosic biomass model components blend with bituminous coal. *Bioresour. Technol.* **2014**, *169*, 220−228.
(40) Wang, B.; Xu, F.; Zong, P.; Zhang, J.; Tian, Y.; Qiao, Y. Effects of heating rate on fast pyrolysis behavior and product distribution of Jerusalem artichoke stalk by using TG-FTIR and Py-GC/MS. *Renew. Energ* **2019**, *132*, 486−496.
(41) Fushimi, C.; Araki, K.; Yamaguchi, Y.; Tsutsumi, A. Effect of Heating Rate on Steam Gasification of Biomass. 2. Thermogravimetric-Mass Spectrometric (TG-MS) Analysis of Gas Evolution. *Ind. Eng. Chem. Res.* **2003**, *42* (17), 3929−3936.
(42) Dai, G.; Wang, G.; Wang, K.; Zhou, Z.; Wang, S. Mechanism study of hemicellulose pyrolysis by combining in-situ DRIFT, TGA-PIMS and theoretical calculation. *Proc. Combust Inst* **2021**, *38* (3), 4241−4249.
(43) Yang, H.; Yan, R.; Chen, H.; Zheng, C.; Lee, D. H.; Liang, D. T. In-Depth Investigation of Biomass Pyrolysis Based on Three Major Components: Hemicellulose, Cellulose and Lignin. *Energy Fuels* **2006**, *20* (1), 388−393.
(44) Cao, J.; Xiao, G.; Xu, X.; Shen, D.; Jin, B. Study on carbonization of lignin by TG-FTIR and high-temperature carbonization reactor. *Fuel Process. Technol.* **2013**, *106*, 41−47.
(45) Vyazovkin, S.; Burnham, A. K.; Criado, J. M.; Pérez-Maqueda, L. A.; Popescu, C.; Sbirrazzuoli, N. ICTAC Kinetics Committee recommendations for performing kinetic computations on thermal analysis data. *Thermochim. Acta* **2011**, *520* (1), 1−19.
(46) Xu, F.; Wang, B.; Yang, D.; Ming, X.; Jiang, Y.; Hao, J.; Qiao, Y.; Tian, Y. TG-FTIR and Py-GC/MS study on pyrolysis mechanism and products distribution of waste bicycle tire. *Energy Convers. Manag* **2018**, *175*, 288−297.
(47) Brachi, P.; Santes, V.; Torres-Garcia, E. Pyrolytic degradation of spent coffee ground: A thermokinetic analysis through the dependence of activation energy on conversion and temperature. *Fuel* **2021**, *302*, 120995.
(48) Alhumade, H.; da Silva, J. C. G.; Ahmad, M. S.; Çakman, G.; Yıldız, A.; Ceylan, S.; Elkamel, A. Investigation of pyrolysis kinetics and thermal behavior of Invasive Reed Canary (Phalaris arundinacea) for bioenergy potential. *J. Anal Appl. Pyrolysis* **2019**, *140*, 385−392.
(49) Zhang, Z.; Duan, H.; Zhang, Y.; Guo, X.; Yu, X.; Zhang, X.; Rahman, M. M.; Cai, J. Investigation of kinetic compensation effect in lignocellulosic biomass torrefaction: Kinetic and thermodynamic analyses. *Energy* **2020**, *207*, 118290.
(50) Du, Z.; Hu, B.; Ma, X.; Cheng, Y.; Liu, Y.; Lin, X.; Wan, Y.; Lei, H.; Chen, P.; Ruan, R. Catalytic pyrolysis of microalgae and their three major components: Carbohydrates, proteins, and lipids. *Bioresour. Technol.* **2013**, *130*, 777−782.

https://doi.org/10.1021/acsomega.1c06363
ACS Omega 2022, 7, 10144−10155